Available online at www.sciencedirect.com
SCIENCE DIRECT
Journal of Molecular Catalysis A: Chemical 255 (2006) 260–268
JOURNAL OF MOLECULAR CATALYSIS A: CHEMICAL
www.elsevier.com/locate/molcata

Photocatalytic activity of epoxide sol–gel derived titania transformed into nanocrystalline aerogel powders by supercritical drying

Lin Chen [a], Jian Zhu [a], Yong-Mei Liu [a], Yong Cao [a,*], He-Xing Li [b], He-Yong He [a], Wei-Lin Dai [a], Kang-Nian Fan [a]

[a] *Department of Chemistry and Shanghai Key Laboratory of Molecular Catalysis and Innovative Materials, Fudan University, Shanghai 200433, PR China*
[b] *Department of Chemistry, Shanghai Normal University, Shanghai 200234, PR China*

Received 14 December 2005; received in revised form 18 April 2006; accepted 20 April 2006
Available online 22 May 2006

Abstract

Nanocrystalline aerogel TiO_2 photocatalysts prepared by a facile epoxide sol–gel synthesis followed by subsequent supercritical drying and thermal processing were studied in regard to their performance in the photocatalytic degradation of phenol. Xerogel TiO_2 catalysts obtained by direct drying were also examined. A variety of techniques including N_2 adsorption, XRD, DRIFTS, TEM, and DR UV–vis were employed to characterize the microstructural and surface properties of the as-obtained aerogel and xerogel TiO_2 samples. It is shown that the aerogel samples showed particular advantage in controlling the microstructural properties in terms of crystallite size, surface area, crystallinity as well as anatase and rutile phase composition, which are responsible for the high activity of these photocatalysts. The aerogel sample obtained by calcination at 650 °C afforded the highest specific activity for photodegradation of phenol, which is also found to be far superior to that of the commercial photocatalyst Degussa P-25.

Keywords: Aerogel TiO_2; Nanocrystalline; Epoxide; Sol–gel; Supercritical drying; Photocatalysis; Phenol degradation

1. Introduction

Heterogeneous photocatalysis utilizing semiconductor materials has recently emerged as an efficient and viable technology for the reduction of global atmospheric pollution and the purification of polluted water [1–5]. The process involves excitation of a semiconducting material by light irradiation, which leads to the generation of electron-hole pairs that have the potential to initiate redox reactions that degrade the contaminant organic compounds. A large variety of oxide and sulfide-based semiconductors capable of photodegradation of the contaminant organic compounds have been reported in the literature [2–4]. Among them, titanium oxide appears to be the most promising and suitable system for photocatalysis owing to its low cost, ease of handling and high resistance to photoinduced decomposition [5]. Extensive researches on the photochemistry and photophysics of TiO_2 have shown that the effective performance of a TiO_2 photocatalyst depends on a number of factors such as the crystal structure, the crystallinity, crystalline size, surface functionality, and most importantly, the surface area and the surface accessibility of the catalyst [6–8].

The use of sol–gel synthesis as a convenient and practical method for the preparation of nanostructured TiO_2 with tailored microstructural properties is well documented in the field of heterogeneous catalysis [9–12]. The advantages of the sol–gel technique are molecular-scale mixing of the components, high purity of the precursor, and homogeneity of sol–gel products with high uniformity of physical, morphological and chemical properties [10,11]. This method is mainly based on the hydrolysis and polycondensation of a metal alkoxide, which ultimately yields hydroxide or oxide under certain conditions [12]. To obtain homogeneous macromolecular oxide networks for qualified nanomaterials in sol–gel processing, control of hydrolysis is essentially important [13]. In the case of titania, titanium alkoxides have been widely used as titanium sources to prepare uniform TiO_2 materials by using alcohol or some other chelating agents to control hydrolysis [14,15]. Of particular recent interest is the surfactant or template-based sol–gel approach [16–18],

* Corresponding author. Tel.: +86 21 65643792/5; fax: +86 21 65642978.
E-mail address: yongcao@fudan.edu.cn (Y. Cao).

1381-1169/$ – see front matter © 2006 Elsevier B.V. All rights reserved.
doi:10.1016/j.molcata.2006.04.043

which can allow the fabrication of ordered mesoporous TiO_2 materials with tunable pore diameters and a high surface area. However, these materials are usually thermally unstable, which greatly compromised their potential applications [18].

Recently, highly porous titania-based aerogels have attracted considerable attention as high performance photocatalysts because of their much larger specific surface areas and higher porosities than conventional sol–gel-derived TiO_2 materials [19,20]. With regard to the synthesis of aerogel materials, the preparation process generally involves two consecutive synthetic procedures comprising an initial sol–gel process followed by subsequent solvent removing step under various supercritical conditions [21]. The main motivation for combining the sol–gel technique with a supercritical drying technology was due to the easily controllable preparation of solid products with interesting textural, chemical and morphological properties [22,23]. In this respect, a number of recent literatures have focused on the development of a variety of high temperature or low temperature supercritical drying methods applicable to the preparation of nanocrystalline titania-based aerogels with optimized photocatalytic activities [24,25]. The most promising results have been achieved by the high-temperature supercritical drying techniques based on alcoholic solvents such as ethanol or isopropanol, which can readily allow the direct fabrication of nanocrystalline anatase TiO_2 aerogel powders highly effective for the photocatalytic degradation of phenolic compounds [26,27].

Concerning the sol–gel process employed for preparing the monolithic wet alcogels subjected to subsequent supercritical drying, titanium alkoxides have been the most frequently used precursors because of their high sol–gel reactivity [27,28]. Recently, a new highly versatile "alkoxide free" sol–gel method using simple inorganic salt precursors has been developed by researchers at Lawrence Livermore National Laboratory [29]. By using epoxides as the gelation agents, this method eliminates the need for the often-difficult preparation and handling of metal alkoxide precursors thus being an attractive complement to traditionally prepared sol–gel materials. A variety of transition, main group and rare earth metal oxide aerogels have been successfully prepared by this method [30–32]. However, to the best of our knowledge, there has been no work dealing with the synthetic preparation of nanocrystalline TiO_2 aerogel materials via the above-mentioned "nonalkoxide sol–gel" method. Moreover, knowledge on the photocatalytic behavior of as well as thermal stability of the TiO_2 aerogel materials obtained by epoxide sol–gel method has not yet been reported.

In the present study, we report that highly photoactive nanocrystalline TiO_2 aerogels with a partial control of the pore-solid architecture and the nanocrystalline phase can be synthesized by supercritical drying of the alcogels formed via a facile epoxide-mediated sol–gel method (Scheme 1) followed by subsequent calcination at elevated temperatures. A number of processing parameters that control the morphology and structural properties of the aerogel TiO_2 samples have been examined. Special attention has been paid to the comparison of the photoactivity and the microstructural properties of the aerogel and xerogel products derived by the epoxide-mediated sol–gel method. A comparison of the photocatalytic properties of the present aerogel/xerogel samples with that of commercial photocatalyst Degussa P-25 was also presented.

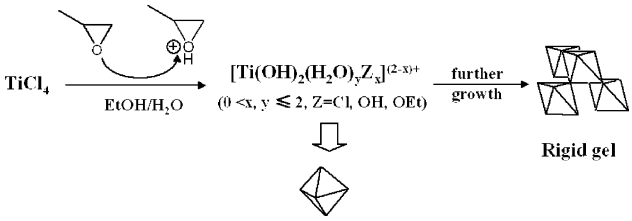

Scheme 1. The reaction scheme proposed for the epoxide-mediated sol–gel process.

2. Experimental

2.1. Sample preparation

The present epoxide sol–gel preparation of TiO_2 gel was based on the synthetic route for preparing Fe_2O_3-based aerogel materials elaborated by Gash et al. [29]. Firstly, titanium chloride ($TiCl_4$, Aldrich, 98%, 1.8 g) was dissolved in absolute ethanol (SCR, 99.85%, 20.0 ml) followed by an immediate addition of 0.51 ml water. After stirring for 15 min, 3.3 g of propylene epoxide (PO) was added drop-by-drop to the titanium-containing alcoholic solution at room temperature under continuous stirring (100 rpm). The titanium/water/epoxide molar ratio was 1/3/6. Within 5–6 min, monolithic, translucent TiO_2 alcogel was obtained. The resulting gel was aged for 12 h at room temperature. The translucent alcogels were then subjected to a series of solvent exchanges in anhydrous ethanol for 3 days.

To obtain the monolithic aerogel from alcogel, we performed drying under supercritical conditions of carbon dioxide ($T_c = 31\,^{\circ}C$, $P_c = 73.8$ bar). When the pore liquid is removed as a gas phase from the interconnected sol–gel network under supercritical conditions (critical-point drying method), the network does not collapse and a low-density aerogel is produced. The alcogel was put into a stainless steel autoclave (150 ml in volume). The solvents present in the alcogel (EtOH and trace amount of H_2O) were replaced with liquid CO_2 and then, the system was brought to above the critical point for 300 min, at a pressure of 80 bar and a temperature of 40 °C. After supercritical drying, off-white monolithic TiO_2 taking the shape of the container was obtained.

Direct drying for obtaining the xerogel powder has been achieved by exposing the solvent-exchanged alcogel to ambient conditions for 24 h followed by air-drying the sample in an oven at 80 °C for 2 more days. To remove most of the organic residues, calcination of the as-obtained aerogel and xerogel samples was carried out in a muffle oven in air at 400, 500, 600, 650 and 700 °C for 4 h, respectively.

Throughout this work, a set of abbreviations is used: TA-AS, TA-400, TA-500, TA-600, TA-650 and TX-700. The T refers to titanium used to form the TiO_2 sample, A to the supercritical drying in carbon dioxide and X the direct drying under ambient

conditions. The heating temperature is indicated at the end of each reference.

2.2. Sample characterization

The textural parameters have been measured using the BET method by N_2 adsorption and desorption at 77 K in a Micromeritics TriStar system. Transmission electron micrographs (TEM) was recorded digitally with a Gatan slow-scan charge-coupled device (CCD) camera on a JEOL 2011 electron microscope operating at 200 kV. The samples for electron microscopy were prepared by grinding and subsequent dispersing the powder in acetone and applying a drop of very dilute suspension on carbon-coated grids. The X-ray powder diffraction (XRD) of the samples was carried out on a Germany Bruker D8Advance X-ray diffractometer using nickel filtered Cu Kα radiation with a scanning angle (2θ) of 10–80°, and a voltage and current of 40 kV and 20 mA. The average size of anatase TiO_2 crystallites was estimated by means of the Scherrer equation from broadening of the (1 0 1) anatase reflection. Estimation of the content of anatase is based on: $X_A = 1/[1 + 1.265 I_R/I_A] \times 100\%$, where I_A is the (1 0 1) peak intensity of anatase, I_R the (1 1 0) peak intensity of rutile, and 1.265 is the scattering coefficient. Diffuse reflectance infrared Fourier transform spectroscopy (DRIFTS) characterization of the catalysts was performed using a Bruker Vector 22 instrument equipped with a Harrick diffuse reflectance cell fitted with KBr windows and a thermocouple mount that allowed direct measurement of the sample temperature. All spectra were collected in nitrogen atmosphere at 150 °C. Diffuse reflection (DR) UV–vis spectra were recorded on a Shimadzu UV 2450 spectrophotometer using a diffuse reflection cell. $BaSO_4$ was used as a reference.

2.3. Photocatalytic degradation of phenol

Photodegradation of phenol in water has been chosen as a test reaction. The laboratory irradiation experiments were performed in a self-constructed photoreactor (see Fig. 1) consisting of a cylindrical quartz flask (diameter 50 mm, length 180 mm) placed in the middle of an internal aluminum-foil lined steel cylinder. The temperature of the suspension system was controlled around 25 ± 0.5 °C by circulating cooling water. The used source of UV irradiation was two high-pressure mercury lamps enclosed in a glass filter bulb (HPW, 150 W, Philips) whose emission consists to 93% of 365 nm radiation.

Briefly, an amount of 400 mg of the catalyst was dispersed in 300 ml of the phenol (SCR, 99%) aqueous solution ($C = 0.60$ mmol/l). Before use, the TiO_2 suspension was sonicated for 5 min with a sonicator (Brandson, 240 W, 2 kHz). The pH of the resulting suspension was taken as the initial value and under the experiment was kept at 7.0. The prepared suspension was then magnetically stirred for about 30 min under the condition of oxygen bubbling (50 ml/min) in dark to achieve the adsorption/desorption equilibrium. At regular irradiation intervals, the dispersion was sampled (ca. 1 ml), centrifuged and subsequently filtered through a Millipore filter to remove the photocatalyst sample before the HPLC analysis (5 μm, 50 mm × 4.6 mm, Akzonobel KR100-5C18 ODS column, 50% methanol–water mobile phase, UV detector), from which the phenol degradation yield (%) was calculated by comparing the initial content of phenol in the solution.

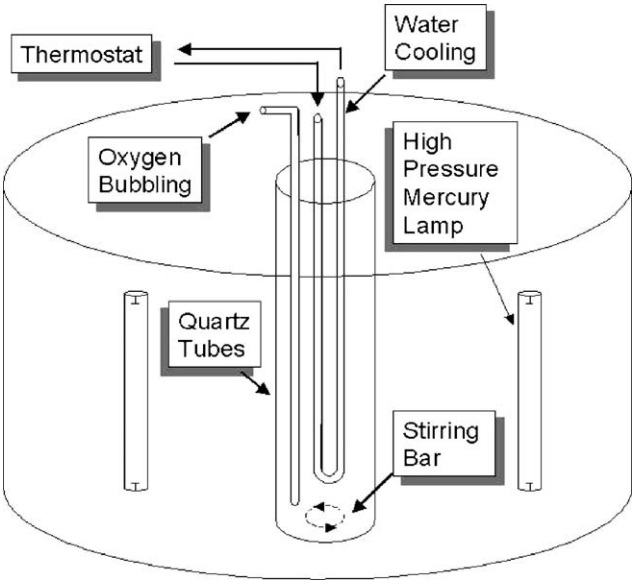

Fig. 1. Experimental setup for the photoreactor.

The kinetic analysis was performed in terms of modified (for solid–liquid reactions) Langmuir–Hinshewood kinetic treatment [33–35]. This mechanism results in pseudo-first-order kinetics at the photostationary state. The reaction order constant for photodegradation of phenol in water suspension was calculated.

3. Results

3.1. Physicochemical features of the TiO_2 samples

The specific surface area (S_{BET}) and the cumulative pore volume of the as-synthesized titania aerogel sample have been found to be 464 $m^2\ g^{-1}$ and 2.06 $cm^3\ g^{-1}$, respectively, consistent with the previous reports of alkoxides-derived titania aerogels [20,36,37]. The N_2 adsorption/desorption isotherms as well as the pore size distribution of the as-synthesized aerogel sample unambiguously reveal the characteristic three-dimensional foam-like structure of the aerogel materials. Table 1 shows the variations of the surface area and pore volume for the aerogel and xerogel samples as a function of calcination temperature. It is seen that the S_{BET} of the calcined aerogel TiO_2 is significantly lower than that of the as-synthesized sample and decreases with increasing calcination temperature. This decreasing trend is also shown by the data for the xerogel samples. Notice that the S_{BET} of all the aerogel catalysts are much higher than their xerogel counterparts in the whole range of temperature studied. The results in Table 1 also clearly indicate that the calcination at elevated temperatures would cause a continuous loss of the pore volume of the aerogel materials, but it remains significantly higher than the pore volumes of xerogel materials prepared by

Table 1
Physicochemical and photocatalytic properties of the aerogel and xerogel TiO_2 materials obtained by the epoxide sol–gel method

Sample (nm)	S_{BET}[a] ($m^2\ g^{-1}$)	V_p[a] ($cm^3\ g^{-1}$)	D_p[a] (nm)	d[b] (nm)	Anatase:rutile [c]	Degradation yield[d] (%)
TA-AS	464	2.06	23.2	–	–	–
TA-400	116	0.62	9.0	8.6	100:0	88.7
TA-500	99	0.5	14.9	11.8	100:0	74.6
TA-600	64	0.4	18.3	16.9	95:5	86.9
TA-650	36	0.25	23.5	22.0	72:28	91.9
TA-700	5	0.07	30	–	4:96	4.76
TX-AS	276	0.042	2.1	–	–	–
TX-400	57	0.147	9.0	12.9	100:0	68.6
TX-500	34	0.107	8.9	16.8	100:0	59.0
TX-600	7.9	0.038	10.9	28.6	95:5	11.4
TX-650	2.5	0.013	6.5	34.7	30:70	4.75
TX-700	0.9	0.002	23.1	–	0:100	0
P-25	55	0.20	20	20.0	70:30	82.2

[a] BET surface area (S_{BET}), average pore volume (V_p) and average pore diameter (D_p) of the aerogel and xerogel samples estimated from nitrogen adsorption.
[b] Average crystallite size (d) of anatase titania nanoparticles estimated from Scherrer equation.
[c] Ratio of anatase to rutile based on XRD data.
[d] Percent of degraded phenol after 120 min irradiation time.

the direct drying method. Moreover, one can notice that the effect of the calcination temperature on the specific surface area for the present epoxide-sol–gel derived aerogel TiO_2 material is less dramatic than the reported one for its conventional alkoxide-sol–gel-derived counterpart in the literature [26,27]. It is remarkable that upon calcination at 600 °C, the aerogel sample still presents a large surface area of 64 $m^2\ g^{-1}$, indicating that the original aerogel structure has been well preserved even after a high temperature calcination. Thus, it can be concluded that thermally stable aerogel TiO_2 materials with a high surface area and large pore volume were obtained in the present study.

Fig. 2 compares the XRD patterns of the aerogel and xerogel titania samples prepared by the present epoxide sol–gel method. Both the as-synthesized samples derived by aerogel and xerogel approach are completely amorphous to X-rays, as seen in Fig. 2. After calcination in air at 400 °C for 4 h, the

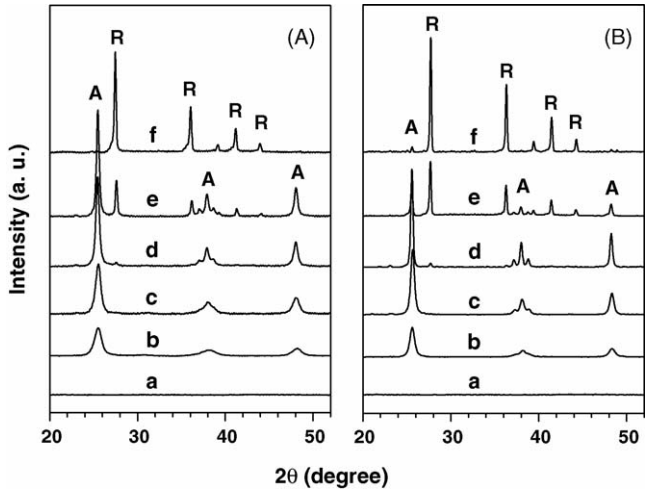

Fig. 2. XRD patterns of the TiO_2 aerogel (A) and xerogel (B) samples calcined at various temperatures: (a) as-prepared; (b) 400 °C; (c) 500 °C; (d) 600 °C; (e) 650 °C; (f) 700 °C. The peaks marked A and R represent the anatase and rutile phase, respectively.

TiO_2 samples exhibited well-defined diffraction peaks characteristic of anatase phase titania. The significant amount of peak broadening observed is due to the nanocrystalline nature of the calcined aerogel. Calcination at elevated temperature in the range of 400–600 °C resulted in a progressive sharpening of the diffraction peaks, indicating a continuous enhancement of the crystallization degree of the anatase phase. From a comparison of the diffraction peaks of anatase in these samples, one can find that the diffraction peaks of anatase for aerogel samples are much broader and lower as compared to their xerogel counterparts, implying a much smaller anatase crystallite size achievable in the aerogel materials. Moreover, several new weak diffraction bands corresponding to the rutile phase were also observed in Fig. 2e, suggesting the occurrence of an appreciable transformation of the anatase to rutile phase in the 650 °C-calcined samples. Further calcination of the samples at temperatures above 650 °C results in the total replacement of anatase by rutile for both aerogel and xerogel materials. The marked difference in the weight ratio of both phases as well as the average crystallite sizes estimated by Scherrer equation for the aerogel and xerogel samples has been tabulated in Table 1.

It is well known that metal oxides obtained by drying the metal hydroxide alcogel precursors under supercritical conditions could often contain a certain amount of carbonaceous residues. Diffuse reflectance FTIR spectroscopy (DRIFTS) has been employed to follow the variation of the surface properties of the epoxide sol–gel derived aerogel and xerogel TiO_2 samples as a function of calcination temperature (Fig. 3). The spectra for all samples show one broad band near 3300 cm^{-1} and another one near 1625 cm^{-1} which correspond to surface-adsorbed water and hydroxyl groups [38]. Absorption in the spectral range of 400–900 cm^{-1} has been assigned to the surface vibrations of the Ti–O bonds [26]. As shown in Fig. 3, the original xerogel and aerogel samples have more surface-adsorbed water and hydroxyl groups than the annealed samples. However, the IR spectra of the original xerogel and aerogel samples (Fig. 3a and d) show significant peaks around ~2931, ~1400 and ~1063 cm^{-1} corre-

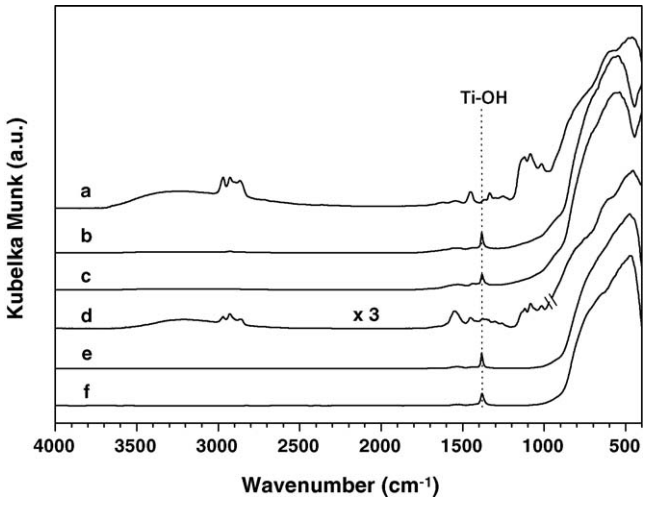

Fig. 3. DRIFT spectra of the xerogel (a–c) and aerogel (d–f) TiO_2 materials: (a and d) as-synthesized, (b and e) calcined at 400 °C for 4 h, and (c and f) calcined at 500 °C for 4 h.

sponding to the remaining organic-moieties on the surface of the as-prepared samples, which practically disappear after thermal treatment. Notice that the spectra for samples TX-400 and TA-400 show much weaker vibrational features around 3000 cm^{-1}, suggesting the presence of only trace amount of carbonaceous residues on the 400 °C-calcined aerogel and xerogel samples. Further calcination at 500 °C results in the total disappearance of the absorption features around 2931 and 1400 cm^{-1} in spectra of Fig. 3c and f, demonstrating unambiguously the clean surface nature for the aerogel and xerogel sample calcined at 500 °C for 4 h. At the same time, absorption peaks relative to Ti–OH bonds (nearly 1385 cm^{-1}) were also observed for the calcined aerogel and xerogel samples [39]. Such Ti-bonded OH groups are favorable for generating and maintaining the photocatalytic activity of crystalline TiO_2 materials [40].

Transmission electron microscopy was used to further examine the particle size and morphology of the aerogel and xerogel TiO_2 samples. An extended nanoparticulate network showing an airy sponge like morphology is observed for the as-prepared aerogel TiO_2 sample (Fig. 4a), in sharp contrast to the highly contracted porous network as identified for the as-synthesized xerogel sample (Fig. 4d). Following calcination at 400 °C, loosely aggregated spherical nanoparticles with the similar particle size around 8–10 nm were observed for the aerogel sample (Fig. 4b), suggesting that the extended network of the original aerogel sample can be partially retained after calcination. After calcination at 650 °C, larger particles (20–30 nm) and even big lumps were observed for the aerogel sample because of the gathering of small particles at high temperature. As a comparison, much larger particles with severe particulate agglomeration can be observed from the TEM images of the calcined xerogel samples (Fig. 4e and f), demonstrating the less thermally stable nature of the xerogel sample obtained by the direct drying method.

Fig. 5 shows the UV–vis diffusion reflectance spectra of the aerogel and xerogel TiO_2 samples prepared by the epoxide sol–gel approach together with that of commercial Degussa P-25. It was obvious that for aerogel TiO_2 materials prepared at temperatures lower than 600 °C, a main UV absorption edge at about 410 nm corresponding to the band gap of ca. 3.03 eV is present. The observed absorption is attributable to the $O^{2+} \rightarrow Ti^{4+}$ charge transfer transition corresponding to the excitation of electrons from the valence band O $2p_\pi$ to the conduction band Ti d_{xy} [41]. For aerogel TiO_2 samples calcined at temperatures higher than 600 °C, a significant red shift of the absorption edge to a lower energy as a consequence of the formation of appreciable amount of rutile phase can be seen (from about 410 to 420–425 nm). Note that the TA-700 sample containing only trace amount of anatase shows the lowest band energy with respect to all other aerogel samples. This is in good accordance with the fact that the rutile has smaller band gap energy than the anatase phase [42]. Moreover, for the TA-650 sample with a similar particle size (ca. 20 nm) and phase composition (ca. 75% anatase and 25% rutile), an evident shift of the absorption edge toward a longer wavelength with respect to that of Degussa P-25 is also identified, indicating that the TA-650 catalyst could absorb energy from a wider range of light than the latter. A similar observation was also made from the xerogel TiO_2 samples calcined at elevated temperatures (inset to Fig. 5).

It should be noted that the UV–vis diffuse reflectance spectrum for Degussa P-25 shows clearly a stronger UV reflection at any wavelength compared to all other samples investigated. Additionally, absorption of light of about 85% was measured for the Degussa P-25 sample from 400 nm down to 200 nm (within the UV range). It appears that the aerogel samples absorbed light also in the visible range above 400 nm, as indicated from the only 80–95% reflection as seen in Fig. 5. Moreover, reflectance at wavelength longer than 400 nm for aerogel samples increases with increasing calcination temperature up to 650 °C, but decreases markedly for TA-700 sample prepared at higher temperatures. It is likely that the reduced UV reflectance (or increase in light absorption) in the visible range as observed for the aerogel samples is a result of light diffusion effect of the aerogel powder during the UV diffuse reflectance measurements [43]. However, the presence of trace amount of residual carbon species may also contribute to some extent to the increase in light absorption in the visible range for the present aerogel samples with calcination temperature lower than 500 °C. Comparison of the diffuse reflectance spectra of the aerogel and the xerogel samples calcined at temperatures of 400–700 °C reveals a much higher reflectance for the aerogel sample at wavelength longer than 400 nm. Taking into account the fact that the xerogel samples calcined at low temperatures may still contain appreciable amount of residual carbon contamination, it is reasonable that an enhanced visible light absorption for the xerogel samples was observed.

3.2. Photocatalytic activity of the TiO_2 samples

The photocatalytic degradation of phenol has been chosen as a model reaction to evaluate the photocatalytic activities of the present aerogel and xerogel catalysts. The apparent kinetics of disappearance of phenol was followed by determining the concentration of the substrate at various time intervals. Table 1

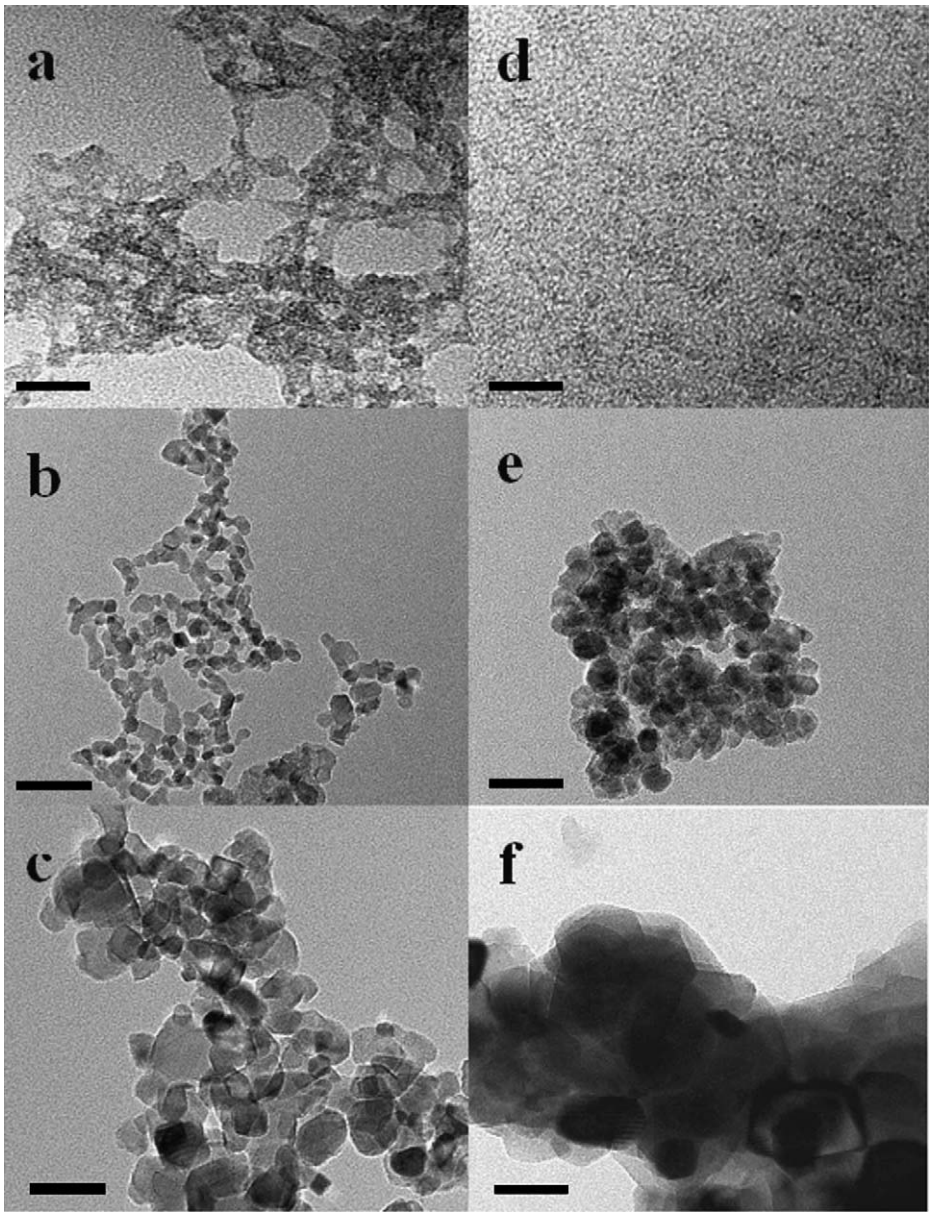

Fig. 4. TEM images of aerogel (a–c) and xerogel (d–f) TiO_2 samples: as-prepared (a and d) and calcined at 400 °C (b and e) and 650 °C (c and f). Scale bar: 50 nm.

presents the phenol degradation yields obtained for all catalyst samples after 120 min of irradiation. All samples showed catalytic activity in phenol degradation reactions depending on the preparation method and the calcination temperature used. It is seen that the photocatalytic activity of the aerogel samples in terms of photodegradation conversion of phenol is much higher than that of the xerogel samples. All aerogel samples, except the TA-700 sample, revealed a photocatalytic activity quite comparable with that of the commercial photocatalyst Degussa P-25. In particular, the highest catalytic activity was achieved with the TA-650 sample obtained by calcination of the fresh aerogel sample at 650 °C for 4 h. It is remarkable that an effective removal of phenol as high as about 92% could be achieved over the aerogel TA-650. By contrast, the Degussa P-25 can only reach ca. 82% of phenol conversion within the same reaction time.

From Table 1, it is also noticed that the calcination temperature is a key parameter strongly influencing the photoactivity of both the aerogel and xerogel samples. In the case of the xerogel samples, the highest catalytic activity was observed for the TX-400 sample obtained by an initial calcination of the as-prepared xerogel sample at 400 °C. With increasing calcination temperature from 500 to 700 °C, a rapid decrease in the activities was observed for the xerogel samples. This is most likely due to a dramatic loss in the specific surface area accompanied by a significant sintering as observed for these xerogel samples. Nevertheless, a significantly different behavior of the photocatalytic activity as a function of calcination temperature has been observed in the aerogel samples. While the TA-400 catalyst prepared at 400 °C showed a high photocatalytic activity for the photodegradation of phenol, the aerogel catalyst prepared at 500 °C showed very low photocatalytic activity possibly due

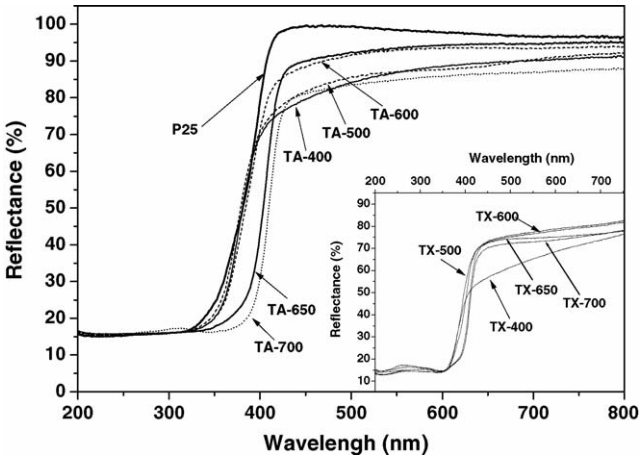

Fig. 5. Diffuse reflectance UV–vis spectra of various aerogel and xerogel (inset) samples obtained by the epoxide sol–gel method. For comparison purposes, the spectrum of the commercial photocatalyst of Degussa P-25 powder is also included.

Table 2
The kinetic parameters of the aerogel, xerogel and Degussa P-25 TiO_2 samples for the photodegradation of phenol

Sample	k_{obs}[a] (min^{-1} g^{-1})	r_0[b] ($\mu mol\,l^{-1}$ min^{-1} g^{-1})	R_0[c] ($\mu mol\,l^{-1}$ min^{-1} m^{-2})
TA-400	0.37	233	2.01
TA-500	0.24	152	1.53
TA-600	0.34	217	3.38
TA-650	0.41	259	7.19
TA-700	0.008	5.1	1.02
TX-400	0.19	122	2.15
TX-500	0.15	94	2.78
TX-600	0.02	13	1.61
TX-650	0.008	5.1	2.04
TX-700	0	0	0
P-25	0.30	189	3.43

[a] The apparent first order reaction rate constants (k_{obs}).
[b] The initial reaction rates per used mass (r_0).
[c] The initial reaction rates per unit surface area (R_0).

to a decrease in the specific surface area. However, the aerogel catalysts prepared at higher temperatures of 600 and 650 °C with even smaller surface areas were found to be more highly active not only for their well-crystalline structure but also due to the varied composition ratio of anatase and rutile as with P-25. Among all the aerogel catalysts tested, the TA-700 sample, which has very low specific surface area and is composed of large crystallites in the rutile phase, affords the lowest catalytic activity for the photocatalytic degradation of phenol.

To gain a further insight into the kinetic aspect of the phenol removal from its aqueous solution in the presence of the aerogel and xerogel catalysts, the plot of the natural logarithm of residual concentration of phenol in reaction solution versus UV irradiation time is shown in Fig. 6. For comparison, the kinetic plot obtained on Degussa P-25 is also included. The straight line obtained shows that the degradation of phenol follows the first order kinetics. To make the further mathematic inferences clear, all the relating kinetic parameters, such as the reaction rate constants (k_{obs}), and calculated initial reaction rates per used mass (r_0) and per unit surface area (R_0) of the lines in Fig. 6, are all reported in Table 2. Again, it is seen that the photocatalytic activity of the aerogel samples is much higher than their xerogel counterparts, and the aerogel samples with the calcination temperature in the range of 400–800 °C are quite comparable to that of the Degussa P-25. Noticeably, the photocatalytic activity in terms of the initial reaction rates per unit surface area (R_0) obtained on the aerogel sample calcined at 650 °C (TA-650) is found to be far superior to that of the Degussa P-25, demonstrating the intrinsic high performance of the TA-650 sample for the photocatalytic degradation of phenol.

4. Discussion

Previous investigations concerning the synthesis of aerogel TiO_2 materials using conventional sol–gel chemistry revealed that in order to obtain uniform titania alcogels with highly

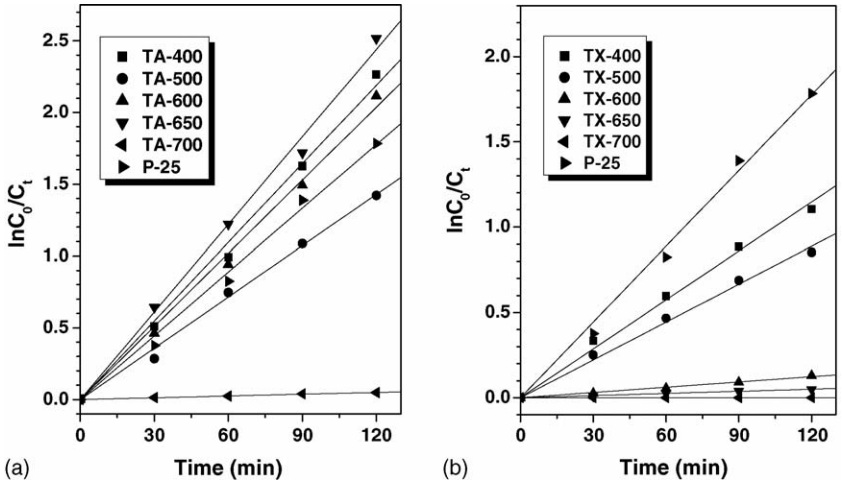

Fig. 6. Natural logarithm plot of the removal of phenol (C_t is the concentration of phenol at a given instant and C_0 is the initial concentration) with (a) aerogel and (b) xerogel TiO_2 photocatalysts. The plot obtained on Degussa P-25 is also included.

cross-linked networks for supercritical processing, the control of hydrolysis of titanium alkoxides by using alcohols or a number of chelating agents is essentially important [14,15]. The present work shows that highly photoactive nanocrystalline TiO_2 aerogel materials can be successfully synthesized via a facile "nonalkoxide sol–gel" method by using epoxide as the gelation agents, followed by subsequent supercritical drying in carbon dioxide and calcination at elevated temperatures. It is important to note that the present "epoxide-mediated nonalkoxide sol–gel" method can allow the easy and convenient generation of high quality monolithic alcogels with homogeneous macromolecular oxide networks by using more easily available titanium chloride ($TiCl_4$) as the titanium precursor, thus providing a new facile and straightforward method for the preparation of nanostructured titania materials with effective control of the pore-solid architecture, the crystallite size, and the resulting photocatalytic properties.

It is known in the literature that the photoactivity of TiO_2 catalysts is influenced by a number of microstructural parameters of the materials, such as particle size, crystalline quality, morphology, and specific surface area as well as porosity [44]. Generally, it is widely accepted that highly porous nanocrystalline TiO_2 materials possessing an open pore-solid architecture with a high surface area and a high volume can lead to a much better performance in photocatalytic reaction [20,24,26]. In the present work, we have unambiguously demonstrated that the present epoxide sol–gel method can allow the convenient generation of new type TiO_2 aerogel catalysts with good thermal stability and high specific surface area. As can be seen in Table 1, the fresh as-prepared aerogel has a large S_{BET} about 464 $m^2\ g^{-1}$. After thermally processed at 400 °C for 4 h, the aerogel TiO_2 still possesses a high value of 100 $m^2\ g^{-1}$, which is almost twice that of commercial photocatalyst Degussa P-25. From the TEM images as shown in Fig. 4, one can see that the characteristic aerogel structure was retained even after high temperature calcination, though agglomeration occurred to some extent. The well-preserved pore-solid structure and relatively high specific surface area may facilitate the mass transport of the reactants, which is believed to play a key role in obtaining the superior performance of the TA-samples during the photocatalytic degradation of phenol.

On the other hand, it is well known that the crystalline structure also plays a very important role in the activity of catalyst in heterogeneous photocatalysis [45]. To establish a reasonable correlation between the catalytic performance and the active phase, an attempt is made in the last column of Table 2 to compare the areal catalytic rates or catalytic rates based on a unit catalyst surface area. It is noticeable that the initial areal rates are in the same order as the massive reaction rates within the series of the aerogel and xerogel samples. However, the areal catalytic rate of the most active TA-650 sample containing 72% anatase and 28% rutile is found to be more than twice that of the commercial photocatalyst Degussa P-25, indicating the presence of powerful synergy between the nanoparticles of anatase and rutile TiO_2 for the enhanced intrinsic activity in the photocatalytic degradation of phenol. Note that the commercial Degussa P-25 itself is also a biphasic TiO_2 powder, and the synergetic effect between the contacting anatase and rutile particles has been the main focus of a number of recent literature work [46–48]. While further work is needed to fully understand the mechanism of the improved synergic effect between highly active anatase and less active rutile phases, it is generally believed that this positive effect is related to the strong interaction between the two TiO_2 phases [45,47,48]. Due to the difference in Fermi levels of anatase and rutile TiO_2, the holes or electrons created in one phase may flow into the other phase, which can effectively enhance the photocatalytic activity by reducing the negative charge recombination [48].

Based on the present investigation, it is clear that the superior photocatalytic performance of the epoxide sol–gel derived nanocrystalline TiO_2 aerogel catalysts can be attributed to a favorable combination of the specific surface area, the crystalline size, as well as the phase structure. Noteworthy is that the most active catalyst TA-650 prepared by the present epoxide sol–gel method, which contains 72% anatase and 28% rutile and has a relatively low surface area (ca. 36 $m^2\ g^{-1}$), exhibited much higher specific photocatalytic activity as compared to commercial Degussa P-25 with a similar phase composition. Previous investigations concerning the crystalline structure of TiO_2-based photocatalysts for the photocatalytic degradation of organic pollutants have revealed that the formation of "catalytically active" hetero junctions between the anatase and rutile TiO_2 particles is always associated with a high activity of the catalyst [45–48]. In this respect, it is possible to design and develop new efficient TiO_2-based photocatalyst systems with an optimal contact of the anatase and rutile TiO_2 particles by engineering the anatase/rutile interfacial properties.

5. Conclusions

In the present work, we have successfully demonstrated that highly photoactive nanocrystalline TiO_2 aerogel photocatalysts with a high surface area and a favorable three-dimensional open porosity can be obtained by a facile epoxide sol–gel method followed by subsequent supercritical drying and thermal processing steps. The influence of heat treatment (from 400 to 700 °C) on the microstructural and photocatalytic properties of the as-obtained aerogel catalysts has been shown for the first time. All these materials show high photocatalytic activity in photodegradation of phenol, the aerogel TiO_2 sample calcined at 650 °C being far superior to that of the commercial photocatalyst Degussa P-25. The comparative study of the aerogel and xerogel TiO_2 samples obtained by supercritical drying and direct drying has shown a much higher activity of the aerogel samples due to a higher surface area and more effective control of the crystallite size and nanocrystalline phase.

Acknowledgments

The financial supports from National Natural Science Foundation of China (Grant Nos. 20473021, 20503005, 20421303, and 20407006), the National Key Basic Research Program (Grant No. 2003CB615807) and the Research Fund for the Doctoral Program of Higher Education (Grant No. 20050246071) are gratefully acknowledged.

References

[1] A. Fujishima, T.N. Rao, D.A. Tryk, J. Photochem. Photobiol. C 1 (2000) 1.
[2] H. Takayuki, B. Yoko, J. Colloid Interf. Sci. 288 (2005) 513.
[3] N. Daneshva, D. Salary, A.R. Khataee, J. Photochem. Photobiol. A 162 (2004) 317.
[4] K. Maeda, T. Takata, M. Hara, N. Saito, Y. Inoue, H. Kobayashi, K. Domen, J. Am. Chem. Soc. 172 (2005) 121.
[5] A.L. Linsebigler, G.Q. Lu, J.T. Yates Jr., Chem. Rev. 95 (1995) 735.
[6] T.Y. Peng, D. Zhao, K. Dai, W. Shi, H. Kazuyuki, J. Phys. Chem. B 109 (2005) 4947.
[7] H.Z. Zhang, J.F. Banfield, J. Phys. Chem. B 104 (2000) 3481.
[8] A.C. Pierre, G.M. Pajonk, Chem. Rev. 102 (2002) 4243.
[9] K.H. Santo, M. Fichtner, K. Schubert, Appl. Catal. A 220 (2001) 79.
[10] Z.R. Tian, J.A. Voigt, J. Liu, B. Mckenzie, H. Xu, J. Am. Chem. Soc. 125 (2003) 12384.
[11] J.M. Wu, T.W. Zhang, Y.W. Zeng, S. Hayakawa, K. Tsuru, A. Osaka, Langmuir 21 (2005) 6995.
[12] L.L. Hench, J.K. West, Chem. Rev. 90 (1990) 33.
[13] E.L. Crepaldi, G.J. Soler-Illia, D. Grosso, F. Cagnol, F. Ribot, C. Sanchez, J. Am. Chem. Soc. 125 (2003) 9770.
[14] M. Niederberger, M.H. Bartl, G.D. Stucky, Chem. Mater. 14 (2002) 4364.
[15] H. Kisch, L. Zang, C. Lange, W.F. Maier, C. Antonius, D. Meissner, Angew. Chem. Int. Ed. 37 (1998) 3034.
[16] B.Z. Tian, H.F. Yang, X.Y. Ying, S.H. Xie, C.Z. Yu, J. Fan, B. Tu, D.Y. Zhao, Chem. Commun. 17 (2002) 1824.
[17] J.H. Lee, I.C. Leu, M.C. Hsu, Y.W. Chung, M.H. Hong, J. Phys. Chem. B 109 (2005) 13056.
[18] J.C. Yu, X. Wang, X. Fu, Chem. Mater. 16 (2004) 1523.
[19] L.K. Campbell, B.K. Na, E.I. Ko, Chem. Mater. 4 (1992) 1329.
[20] G. Dagan, M. Tomkiewicz, J. Phys. Chem. 97 (1993) 12651.
[21] H.G. Gesser, P.C. Goswami, Chem. Rev. 89 (1989) 765.
[22] H. Hirashima, C. Kojima, K. Kohama, H. Imai, V. Balek, H. Hamada, M. Inaba, J. Non-Cryst. Solids 225 (1998) 153.
[23] S.O. Kucheyev, T. van Buuren, T.F. Baumann, J.H. Satcher, T.M. Willey Jr., R.W. Meulenberg, T.E. Felter, J.F. Poco, S.A. Gammom, L.J. Terminello, Phys. Rev. B 69 (2004) 245102.
[24] M. Schnieder, A. Baiker, Catal. Today 35 (1997) 339.
[25] P.N. Kapoor, S. Uma, S. Rodriguez, K.J. Klabunde, J. Mol. Catal. A 229 (2005) 145.
[26] Yu.V. Kolen'ko, A.V. Garshev, B.R. Churagulov, S. Boujday, P. Portes, C. Colbeau-Justin, J. Photochem. Photobiol. A: Chem. 172 (2005) 19.
[27] H.-X. Li, G.S. Li, J. Zhu, Y. Wan, J. Mol. Catal. A: Chem. 226 (2005) 93.
[28] Z. Zhu, L.Y. Tsung, M. Tomkiewicz, J. Phys. Chem. 99 (1995) 15945.
[29] A.E. Gash, T.M. Tillotson, J.H. Satcher Jr., J.F. Poco, L.W. Hrubesh, R.L. Simpson, Chem. Mater. 13 (2001) 999.
[30] B.J. Clapsaddle, D.W. Sprehn, A.E. Gash, J. Non-Cryst. Solids 350 (2004) 173.
[31] T.T. Baumann, S.O. Kucheyev, A.E. Gash, J.H. Satcher Jr., Adv. Mater. 17 (2005) 1546.
[32] T.T. Baumann, A.E. Gash, S.C. Chinn, A.M. Sawvel, R.S. Maxwell, J.H. Satcher Jr., Chem. Mater. 17 (2005) 395.
[33] H. Alekabi, P. Demayo, J. Phys. Chem. 90 (1986) 4075.
[34] H. Alekabi, N. Serpone, J. Phys. Chem. 92 (1988) 5726.
[35] T. Hasegawa, P. Demayo, Langmuir 2 (1986) 362.
[36] H. Li, J. Zhu, G. Li, Y. Wan, Chem. Lett. 33 (2004) 574.
[37] H. Tamon, T. Sone, M. Mikami, M. Okazaki, J. Colloid Interf. Sci. 188 (1997) 493.
[38] Y. Tanaka, M. Suganuma, J. Sol–Gel Sci. Technol. 22 (2001) 83.
[39] B.A. Morales, O. Novaro, T. Lopez, E. Sanches, R. Gomez, J. Mater. Res. 10 (1995) 2778.
[40] M.A. Fox, M.T. Dulay, Chem. Rev. 93 (1993) 341.
[41] N. Daude, C. Gout, C. Jounanin, Phys. Rev. B 15 (1977) 3229.
[42] M. Andersson, H. Birkedal, N.R. Franklin, T. Ostomel, S. Boettcher, A.E.C. Palmqvist, G.D. Stucky, Chem. Mater. 17 (2005) 1409.
[43] A. Davydov, in: N.T. Sheppard (Ed.), Molecular Spectroscopy of Oxide Catalyst Surfaces, John Wiley & Sons Ltd., Chichester, 2003, p. 5.
[44] M.R. Hoffman, S.T. Martin, W. Choi, D.W. Bahnemann, Chem. Rev. 95 (1995) 69.
[45] R.I. Bickley, T. Gonzalez-Carreno, J.S. Lees, L. Palmisano, R.J.D. Tilley, J. Solid State Chem. 92 (1991) 178.
[46] M. Yan, F. Chen, J. Zhang, M. Anpo, J. Phys. Chem. B 109 (2005) 8673.
[47] A.K. Datye, G. Riegel, J.R. Bolton, M. Huang, M.R. Prairie, J. Solid State Chem. 115 (1995) 236.
[48] D.C. Hurum, A.G. Agrios, K.A. Gray, T. Rajh, M.C. Thurnauer, J. Phys. Chem. B 107 (2003) 4545.